ISSN 1330-3651 (Print), ISSN1848-6339(Online) https://doi.org/10.17559/TV-20250804002881
Original scientific paper

A Multi-Scale Fusion-Based Method for Ultra-Low-Light Agricultural Image Enhancement

Jun LI*, Zhou WEI, Yining SONG, Shiqiong CHEN, Miao YU, Wenfeng WANG, Chenping ZENG, Yanmeng CHEN

Abstract: Fruits, vegetables, and medicinal herbs are often processed in enclosed spaces with low light. These conditions create uneven lighting, produce dark images, distort colors, and increase noise, all of which make remote monitoring difficult and reduce product quality. This paper uses tobacco leaf curing as an example to introduce a Multi-Scale Fusion-Based Image Enhancement (MSFIE) technique designed to address these problems. Histogram equalization, a CLAHE module, an enhanced dual-gamma correction, and a multi-scale fusion framework are all included in the technique. When combined, these elements improve overall contrast and sharpness, lessen local overexposure, and brighten dark areas. The primary and secondary leaf vein structures are further made clearer by a detail enhancement technique. Experiments on 150 ultra-low-light images demonstrate that MSFIE improves visual quality, brightness uniformity, detail preservation, and color accuracy. Quantitatively, it achieves consistent gains in Shannon entropy, peak signal-to-noise ratio, laplacian-based sharpness, local contrast, frequency-domain sharpness, luminance skewness, and information entropy.

Keywords: color distortion; detail enhancement; low-light image enhancement; MSFIE

1 INTRODUCTION

Agricultural products such as tobacco, fruits, vegetables, and medicinal herbs are often processed in enclosed, low-light environments. These conditions lead to uneven lighting, low image brightness, color distortion, and increased noise [1], which lower product quality and make remote monitoring challenging. Throughout all stages of tobacco leaf drying [2, 3] in kilns including yellowing, color setting, stem dehydration, and leaf dehydration [4] image monitoring is essential. Traditionally, manual inspection has been used for this process, but it is often subjective and inconsistent. As a result, it is challenging to achieve the precision and uniformity required by industry standards. Even with the use of semi-automated kilns, color remains the main measure of curing quality, and farmers still have to check leaf color through observation windows.

Recent advances in digital technologies such as artificial intelligence (AI), the Internet of Things (IoT) [5], and edge computing have made it possible to monitor tobacco color remotely in real time by installing cameras both inside and outside the kilns. These improvements have increased efficiency and reduced the need for manual labor [6]. However, computer vision still faces several challenges in this environment, such as noise, uneven lighting, color distortion, areas that are too bright or too dark, and limited camera coverage. These problems make accurate color detection difficult. To overcome these issues, it is important to use low-light image enhancement techniques to correct color and lighting in kiln images. An overview of the proposed MSFIE architecture is presented in Section 2 (see Fig. 1). Accurate evaluation of tobacco curing stages depends on these improvements. Low-light image enhancement is now a key area of research in image processing, with applications in agriculture, security, and self-driving technologies. Existing approaches include histogram-based methods [7, 8] (efficient but prone to color shifts and noise amplification), Retinex variants [9] (handle uneven illumination yet are parameter-sensitive and computationally heavy), dehazing-inspired models [10] (effective with accurate priors but fragile otherwise), and deep learning methods [11] (high performance but data/compute intensive with limited interpretability). Recent works cover zero-reference curve estimation, transformer-based models [12], and GAN variants [13].

Despite these developments, problems with uneven lighting and strong noises still plague photos of tobacco leaves taken in enclosed, extremely low-light conditions. To solve these problems, we propose a multi-scale fusion-based image enhancement (MSFIE) method for ultra-low-light tobacco images. This method brings together histogram equalization, gamma correction, CLAHE, and detail enhancement. As a result, MSFIE can better capture small color changes during curing, improve overall brightness and sharpness, enhance local contrast, prevent overexposure, and highlight key leaf vein details - while preserving important information.

The main contributions of this work are:

A multi-scale fusion framework that integrates histogram equalization, adaptive dual-gamma correction with cosine boundary blending, CLAHE on the L channel with adaptive clip limit, and edge-aware multi-scale detail enhancement tailored for ultra-low-light agricultural images.

An adaptive weighting strategy that fuses fine/base/coarse details using Laplacian variance, Sobel edge strength, and local contrast, preserving leaf veins while suppressing noise.

A comprehensive evaluation across six lighting scenarios with diverse metrics, plus analysis of metric redundancy and measurement scaling for interpretability.

2 RELATED WORK

Fig. 1 illustrates the overall architecture of MSFIE, highlighting its core modules and data flow. (a) Pipeline with four modules: histogram equalization, gamma correction, CLAHE, and detail enhancement. (b) Adaptive dual-gamma correction. (c) CLAHE on the L channel with adaptive clip limit. (d) Multi-scale detail enhancement and fusion.

Histogram-based methods redistribute global contrast efficiently but can introduce color distortion and noise amplification under severe low light and mixed illumination. Let $H(I)$ denote the histogram of image I. Global HE seeks a monotone mapping T so that the CDF of $T(I)$ approximates a uniform CDF U, i.e., $F_{T(I)}(v) \approx U(v)$. While this increases global contrast, it may amplify sensor noise n when $I = s + n$ and s has narrow dynamic range, yielding $T'(I) \cdot n$ magnification in flat regions.

Retinex-based approaches decompose $I(x)$ into reflectance $R(x)$ and illumination $L(x)$, often via $I(x) = R(x) \odot L(x)$ and $\log I = \log R + \log L$. Estimating L with strong smoothness priors (e.g., weighted TV) enables nonuniform illumination correction, but parameter sensitivity and haloing can occur around high-gradient regions when ∇L is over-smoothed. Computational cost also rises due to iterative optimization or multi-scale filtering.

Dehazing-inspired methods transfer priors (e.g., dark channel, haze-line) to low-light enhancement by modeling $I = J \cdot t + A(1 - t)$ and adjusting t or A after an intensity inversion. Their performance hinges on prior validity; mixed illumination, specular highlights, and sensor noise often violate assumptions, causing color shifts or detail loss. Prior selection and parameter estimation can be computationally demanding.

Deep learning methods including zero-reference curve estimation (e.g., ZeroDCE/ZeroDCE++), transformer-based enhancement, and GAN variants optimize enhancement functions $f_\theta(I)$ from data, often balancing brightness, detail, and noise. However, they require substantial data/compute and may generalize poorly without domain-specific training. Our MSFIE is training-free and differs by combining adaptive dual-gamma with cosine blending, Laplacian-guided CLAHE, and edge-aware multi-scale detail fusion, specifically tuned for ultra-low-light agricultural imagery.

3 MATERIALS AND METHODS

3.1 Overview of the MSFIE Framework

The MSFIE algorithm integrates several low-light image enhancement techniques to maximize their collective benefits. First, histogram equalization globally stretches pixel values, improving overall brightness and contrast. Second, an adaptive dual-gamma correction adjusts gamma parameters for dark and bright regions based on image brightness statistics, enhancing details in shadows, reducing overexposure, and enriching tonal gradation. Third, an improved CLAHE algorithm adaptively boosts contrast in the brightness channel while minimizing local over-enhancement and artifacts through feature analysis. Finally, a multi-scale Gaussian filter extracts texture features at different levels, while edge-aware and content-adaptive weighting sharpen details and control noise. This fusion approach significantly enhances dark areas, expands tonal range, improves structural details, and preserves natural visual quality, resulting in clearer images under extremely low-light conditions.

Fig. 1 shows the MSFIE framework for enhancing extremely low-light tobacco images through multi-scale fusion. The method comprises four modules: Histogram Equalization, Gamma Correction, CLAHE Contrast Enhancement, and Image Detail Enhancement, which together improve contrast, brightness, and local details. Each tobacco image's RGB channel is processed through these modules for comprehensive enhancement.

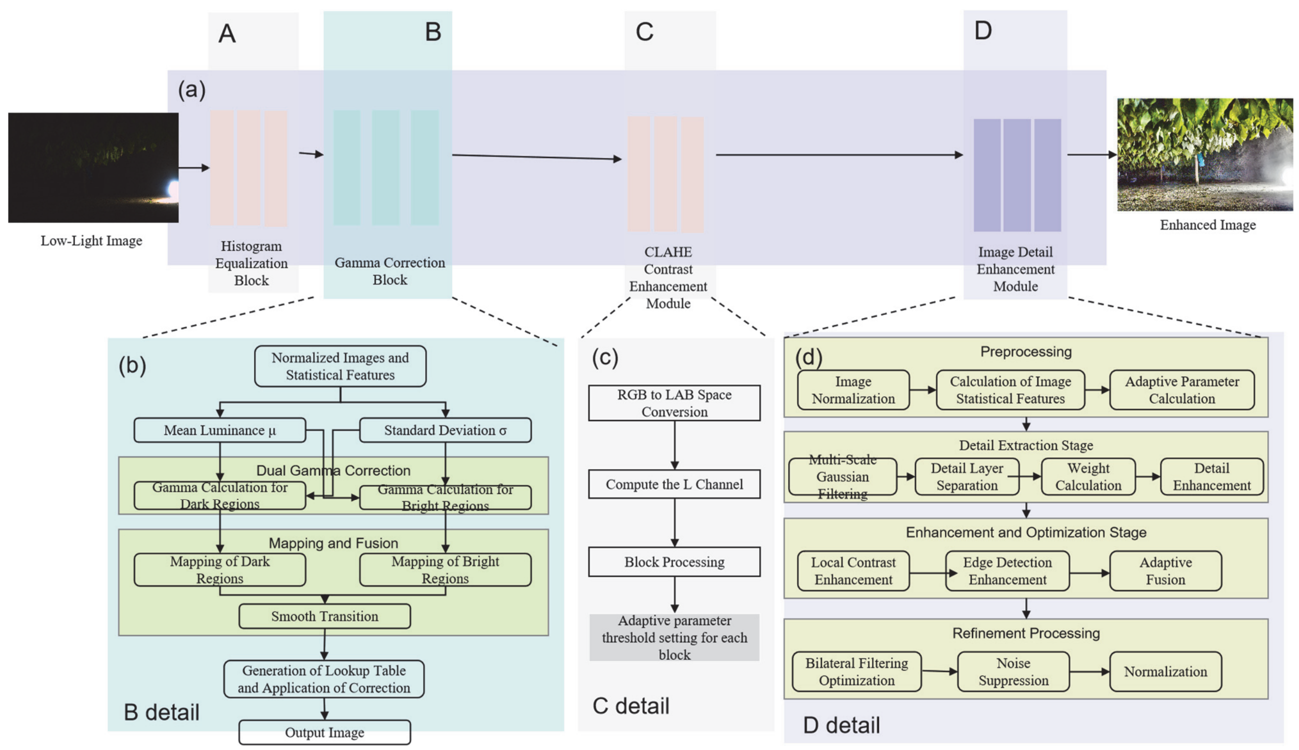

Figure 1 Network framework for low-light image enhancement. (a) The framework of the proposed multi-scale fusion-based method for ultra-low-light tobacco leaf image enhancement (MSFIE) framework, which can be divided into four categories: histogram equalization block, gamma correction block, CLAHE contrast enhancement module, and image detail enhancement module; (b) The framework of the gamma correction block; (c) The framework of the CLAHE contrast enhancement module; and (d) The framework of the image detail enhancement module

Fig. 1a exemplifies an extremely low-light image with a strong light source and details the four stages (A-D) of the process. The Histogram Equalization Block sharpens blurry areas and increases overall contrast. The enhanced dual-gamma correction brightens shadows and reduces overexposure in highlights. The CLAHE module further improves local brightness and contrast, ensuring consistent image quality under different lighting conditions. Finally, the detail enhancement module uses high-frequency filtering to emphasize leaf veins and improve local details.

3.2 Gamma Correction Enhancement

The adaptive dual-gamma correction algorithm separates the image into dark and bright areas based on its brightness distribution. It applies a lower gamma value to dark areas to boost brightness and detail. In bright areas, it uses a higher gamma value to reduce highlights and prevent overexposure. This method improves shadow visibility, preserves highlight structure, and optimizes overall brightness, contrast, and gradation. To formalize the method, we consistently use μ_{norm} , σ_{norm} , and the normalized image $I_{\text{img\_nor}}$ throughout, replacing mixed forms such as $I_{\text{img\_nor}}/I_{\text{im\_nor}}$.

Fig. 1b shows the normalization process for the input image. The gamma values for dark and bright regions are adaptively set using the global brightness mean (μ_{norm}) and standard deviation (σ_{norm}). This targeted enhancement improves shadow detail and avoids highlight overexposure. For each pixel, if its brightness is below the adaptive threshold, it is processed with a lower gamma value (γ_{dark}) as follows:

$$\begin{aligned}\gamma_{\text{dark}} &= \max \\ &(\min(\gamma_{\text{norm}} \times (1-\alpha_{\text{d}} \times \mu_{\text{norm}} + \beta_{\text{d}} \times \sigma_{\text{norm}}), 2.0, 0.5)\end{aligned} \tag{1}$$

where γ_{dark} is the gamma value for dark areas, μ_{norm} and γ_{norm} is the standard gamma value. The coefficients α_{d} and β_{d} represent the weights for brightness and contrast.

The exponential adjustment using a higher gamma value (γ_{bright}) is expressed as follows:

$$\begin{aligned}\gamma_{\text{bright}} &= \max \\ &(\min(\gamma_{\text{norm}} \times (1+\alpha_{\text{d}} \times \mu_{\text{norm}} + \beta_{\text{d}} \times \sigma_{\text{norm}}), 2.5, 1.0)\end{aligned} \tag{2}$$

where γ_{bright} is the gamma value used for bright regions.

The dual-gamma mapping function enables localized, nonlinear enhancement of the image and is defined as follows:

$$\begin{aligned}&I_{(gamma\_1)}(x,y) = \\ &255 \times (I_{\text{he}}(x,y)/255)^{(1/\gamma_{\text{gamma}})}, r_{\text{gamma}} \in \{r_{\text{dark}}, r_{\text{bright}}\}\end{aligned} \tag{3}$$

where x and y represent the row and column coordinates of each pixel. $I_{\text{bright\_gamma}}(x, y)$ indicates the mapped image of the bright or dark regions in $I_{\text{he}}(x, y)$, where $I_{\text{gamma\_1}}(x, y)$ may refer to either $I_{\text{bright\_gamma\_1}}(x, y)$ or $I_{\text{dark\_gamma\_1}}(x, y)$.

To prevent abrupt transitions at the boundary regions, cosine weighting is applied to achieve a smooth transition:

$$\begin{aligned}&I_{\text{gamma}}^{(i)}(x,y) = \\ &w^{(i)} \times I_{\text{dark}_{\text{gamma}_1}}^{(i)}(x,y) + \left(1-w^{(i)}\right) \times I_{\text{bright}_{\text{gamma}_1}}^{(i)}(x,y)\end{aligned} \tag{4}$$

where $w^{(i)}$ represents the weight value of the window function, and i denotes the index of the current image position.

We constrain $r_{\text{dark}} \in [0.5, 2.0]$ and $r_{\text{bright}} \in [1.0, 2.5]$ to balance enhancement and artifact suppression. Wider ranges produced banding and haloing near strong light sources in pilot tests; these bounds yielded the best trade-off across all six lighting scenarios. Eqs. (1) to (4) implement an adaptive dual-gamma scheme: darker pixels are brightened to reveal hidden detail, while bright pixels are compressed to prevent overexposure. Cosine weighting blends boundary regions to avoid visible seams. $I_{\text{gamma}}^{(i)}(x,y)$ refers to the image obtained after smoothing both $I_{\text{dark}_{\text{gamma}_1}}^{(i)}(x,y)$ and $I_{\text{bright}_{\text{gamma\_1}}}^{(i)}(x,y)$.

This smoothing connects the gamma-mapped regions on both sides of the boundary, preventing abrupt changes in pixel intensity caused by discontinuities in the mapping curve, and ensuring a visually natural transition in the image.

3.3 CLAHE Contrast Enhancement

The CLAHE (Contrast Limited Adaptive Histogram Equalization) algorithm improves tobacco leaf images by dividing them into several regions and enhancing each one separately. By doing so, it brings out more detail in dark areas and avoids problems like excessive brightness or visual artifacts that often occur with basic histogram equalization. CLAHE helps achieve better overall contrast, limits overexposure in the brightest areas, and delivers even enhancement across different shades. As a result, shadow regions become clearer and highlights remain natural, leading to a noticeable improvement in image quality.

Fig. 1c illustrates the steps of the CLAHE enhancement process. The procedure begins by converting the dual-gamma corrected BGR color image, $I_{\text{gamma}}(x, y)$, into the LAB color space. The algorithm then targets the L channel for enhancement by dividing it into 8 × 8 smaller blocks and applying contrast-limited histogram equalization to each one. This step increases contrast locally while avoiding added noise or unnatural stretching of brightness:

$$\begin{aligned}&L_{\text{l\_o1}}(x,y) = \\ &\frac{L_{\text{l\_in}}(x,y) - min\left(L_{\text{l\_in}}(x,y)\right)}{\max\left(L_{\text{l\_in}}(x,y)\right) - min\left(L_{\text{l\_in}}(x,y)\right)} \times 255\end{aligned} \tag{5}$$

Here, $L_{\text{l\_o1}}(x,y)$ refers to pixel values processed by the local histogram algorithm, while $L_{\text{l\_in}}(x,y)$ denotes the local values of the input L channel. $\max\left(L_{\text{l\_in}}(x,y)\right)$ and $\min\left(L_{\text{l\_in}}(x,y)\right)$ are the maximum and minimum L channel values within the local region, respectively.

We denote the Laplacian-variance measure by l_{apvar}, computed over the L channel after local equalization. The Laplacian operator [14] is applied to the luminance component to detect edges and details. The variance of the

Laplacian values quantifies the complexity of image details; higher variance indicates richer details, while lower variance suggests a coarser texture. The variance of the Laplacian values for the L channel is calculated as follows:

$$lap_{\mathrm{var}} = \frac{1}{MN}\sum_{x=1}^{M}\sum_{y=1}^{N} \left(\left[\frac{\partial^2 L_{\mathrm{lo1}}(x,y)}{\partial x^2} + \frac{\partial^2 L_{\mathrm{lo1}}(x,y)}{\partial y^2} \right] - \frac{1}{MN}\sum_{x=1}^{M}\sum_{y=1}^{N} \left[\frac{\partial^2 L_{\mathrm{l\_o1}}(x,y)}{\partial x^2} + \frac{\partial^2 L_{\mathrm{l\_o1}}(x,y)}{\partial y^2} \right] \right)^2 \tag{6}$$

Here, lap_{var} denotes the variance of the Laplacian operator over all pixels in the image; $L_{\mathrm{l\_o1}}(x,y)$ represents the image obtained from local histogram equalization of the L channel in the previous step.

The Laplacian variance (lap_{var}) is used to adaptively adjust the $\mathrm{clip_{limit}}$ parameter of CLAHE:

$$clip_{\mathrm{limit}} = \min(40.0,\ 2.0 + \alpha_{\mathrm{lab}} \times \ln(1 + lap_{\mathrm{var}})) \tag{7}$$

Here, $clip_{\mathrm{limit}}$ represents the contrast limiting value, α_{lab} is the scaling factor, and lap_{var} denotes the variance of the Laplacian operator.

When the image contains abundant details (i.e., lap_{var} is large), the $clip_{\mathrm{limit}}$ is increased to enhance contrast. Conversely, when there are fewer details, the $clip_{\mathrm{limit}}$ remains low to avoid noise amplification and over-enhancement. Logarithmic smoothing and a maximum limit are applied to $clip_{\mathrm{limit}}$ to ensure stable and controlled enhancement, which improves the algorithm's robustness and visual performance across different scenarios. The Laplacian variance lap_{var} measures edge density (detail richness). We map lap_{var} to an adaptive clip limit via a logarithmic function to increase contrast in detail-rich areas while capping contrast in smooth regions to avoid noise amplification. By adaptively adjusting $clip_{\mathrm{limit}}$, a higher cut-off strength is used for detail-rich regions to suppress noise, while a lower enhancement is applied in less detailed areas to prevent artifacts caused by excessive contrast.

Since CLAHE can cause abrupt luminance changes at block boundaries, bilinear interpolation is applied to the processed luminance image (L channel). This uses a weighted average of neighboring pixels to smooth the grayscale values and effectively eliminate block artifacts:

$$\left[x'\ y'\right] = \left[m_{11}\ m_{12}\ m_{13}\ m_{21}\ m_{22}\ m_{23}\right] \cdot \left[x\ y\ 1\right] \tag{8}$$

We apply standard bilinear interpolation across CLAHE tiles to smooth boundaries and prevent block artifacts; Eq. (8) denotes this interpolation in compact form.

3.4 Image Detail Enhancement

Image detail enhancement is achieved using multi-scale Gaussian filtering with adaptive weighting to effectively separate and amplify details across different spatial scales. Multi-scale Gaussian differences isolate fine-, base-, and coarse-scale structures; Sobel-based edge weights and local contrast emphasize salient boundaries, while bilateral filtering suppresses noise. This method highlights key content by extracting edges and enhancing both structural and textural features. The algorithm further adapts to regional differences, enabling targeted feature optimization. Local contrast enhancement improves the visual quality of regions of interest, while adaptive bilateral filtering based on local variance suppresses noise yet preserves important details. Together, these techniques significantly enrich and clarify details in flue-cured tobacco leaf images.

Fig. 1d outlines the enhancement process. The image is first normalized to the [0, 1] range. Global and local standard deviations are calculated to dynamically adjust detail weights, allowing the algorithm to adapt to varying image characteristics. Multi-scale structures are generated using Gaussian blur with varying σ values, and high-frequency details are isolated by subtracting the blurred images from the original. Edge information is extracted using the Sobel operator [15], and a local contrast enhancement model based on edge correlation further refines texture and boundary clarity. Details from all scales are combined via linear weighting and merged with global contrast enhancement results, balancing detail and brightness variations. Finally, bilateral filtering with adaptive parameters effectively reduces noise and smooths texture transitions, ensuring natural and artifact-free results.

The detail enhancement weight, ω_{detail}, governs adaptive parameter adjustment. It is computed by first taking the difference between the Gaussian-blurred and normalized images, and then calculating the local standard deviation ($\sigma_{\mathrm{im\_nor}}$) of this difference to quantify local detail variation. Based on this measure, ω_{detail} is defined as follows:

$$\omega_{\mathrm{detail}} = 1 + \frac{\sqrt{\frac{1}{M \times N} \times \sum_{x=0}^{M-1}\sum_{y=0}^{N-1}\left(I_{\mathrm{gau}}\left(x,y,\sigma_{\mathrm{im\_nor}}\right) - I_{\mathrm{im\_nor}}(x,y) - \frac{1}{M \times N} \times \sum_{i=1}^{M\times N}\left[I_{\mathrm{gau}}^{(i)}(x,y) - I_{\mathrm{im\_nor}}^{(i)}(x,y) \right] \right)^2}}{\sigma_{\mathrm{im\_nor}}} \tag{9}$$

Here, ω_{detail} denotes the adaptive weight of the difference image $I_{\mathrm{diff}}(x, y)$; M and N represent the width and height of $I_{\mathrm{diff}}(x, y)$, respectively; σ_{diff} refers to the local standard deviation of $I_{\mathrm{diff}}(x, y)$; $I_{\mathrm{gauss}}\left(x, y, \sigma_{\mathrm{im\_nor}}\right)$ is the Gaussian-transformed version of the original normalized image $I_{\mathrm{im\_nor}}(x, y)$; and $\sigma_{\mathrm{im\_nor}}$ denotes the standard deviation of $I_{\mathrm{im\_nor}}(x, y)$.

Gaussian blurring is applied to the original image using varying standard deviations:

$$I_{\text{gau}}\left(x,y,\sigma_{\text{im\_nor}}\right)=\left(\frac{1}{2}\pi\sigma_{\text{im\_nor}}\right)\mathrm{e}^{-\frac{x^2+y^2}{2\sigma_{\text{im\_nor}}^2}} \tag{10}$$

Here, $I_{\text{gau}}\left(x,y,\sigma_{\text{im\_nor}}\right)$ denotes the Gaussian-transformed image of the original normalized image $I_{\text{img\_nor}}(x, y)$, and $\sigma_{\text{im\_nor}}$ represents the standard deviation of $I_{\text{img\_nor}}(x, y)$.

The algorithm divides the image structure information into three scales: fine, base, and coarse. A smaller $\sigma_{\text{im\_nor}}$ value emphasizes fine details, while a larger value retains the structural contours of the image.

When local variations in the image are significant - that is, detail is abundant and there is a distinct difference from the overall contrast - the detail enhancement weight ω_{detail} is greater than 1, which highlights the texture details. Conversely, if local and global variations are similar or insignificant, ω_{detail} approaches 1, thereby reducing enhancement to prevent excessive noise amplification or artifact generation in uniform regions, ensuring the authenticity and naturalness of the image. For stability and control, ω_{detail} is constrained to the range [1.0, 2.0] to filter out outliers and prevent oversharpening or structural distortion due to excessively high weights. This cap prevents oversharpening, ringing, and structural distortion around strong edges.

Finally, the original image is subtracted from the fine-, base-, and coarse-scale Gaussian-blurred versions to extract high-frequency details, small-scale textures, and large-scale structural features, respectively. The fine-scale detail calculation formula is:

$$\begin{aligned}&I_{\text{detail\_f}}\left(x,y\right)=\\&\omega_{\text{detail}}\times I_{\text{im\_nor}}\left(x,y\right)+\left(1-\omega_{\text{detail}}\right)\times I_{\text{gau}}\left(x,y,\sigma_{\text{im\_nor}}/3\right)\end{aligned} \tag{11}$$

The base-scale detail calculation formula is:

$$\begin{aligned}&I_{\text{detail\_b}}\left(x,y\right)=\\&\omega_{\text{detail}}\times I_{\text{im\_nor}}\left(x,y\right)+\left(1-\omega_{\text{detail}}\right)\times I_{\text{gau}}\left(x,y,\sigma_{\text{im\_nor}}\right)\end{aligned} \tag{12}$$

The coarse-scale detail formula is:

$$\begin{aligned}&I_{\text{detail\_c}}\left(x,y\right)=\\&\omega_{\text{detail}}\times I_{\text{im\_nor}}\left(x,y\right)+\left(1-\omega_{\text{detail}}\right)\times I_{\text{gau}}\left(x,y,\sigma_{\text{im\_nor}}*3\right)\end{aligned} \tag{13}$$

Here, $I_{\text{detail\_f}}\left(x,y\right)$, $I_{\text{detail\_b}}\left(x,y\right)$, and $I_{\text{detail\_c}}\left(x,y\right)$ represent the fine-scale, base-scale, and coarse-scale detail images, respectively, while Igau denotes the Gaussian-blurred version of the Iimg image.

The Sobel operator is used to compute image gradients in the x and y directions, reflecting edge strength. After normalizing the extracted results, the edge strength weight is given by:

$$\omega_{\text{edge}}\left(x,y\right)=\frac{\sqrt{G_x^2\left(x,y\right)+G_y^2\left(x,y\right)}}{\max\left(\sqrt{G_x^2\left(x,y\right)+G_y^2\left(x,y\right)}\right)+\varepsilon} \tag{14}$$

Here, $\omega_{\text{edge}}\left(x,y\right)$ denotes the edge weight; ε is a small constant ($1\mathrm{e}^{-6}$) for numerical stability; G_x represents the image gradient in the x direction; and G_y represents the image $I_{\text{im}_{\text{nor}}}\left(x,y\right)$ gradient in the y direction.

Local mean adjustment is used to balance the luminance distribution, while an edge strength modulation factor enhances the contrast of boundaries and textures and suppresses noise amplification in homogeneous regions. To reduce the influence of local mean brightness on the outcome, the algorithm adopts the following contrast enhancement formula:

$$\begin{aligned}&I_{\text{local}_{\text{contrast}}}\left(x,y\right)=\\&\frac{1}{N_{\text{local}}}\times\sum_{i=-k}^{k}\sum_{j=-k}^{k}I_{\text{im\_nor}}\left(x+i,y+j\right)\times\left(1+k\times\omega_{\text{edge}}\left(x,y\right)\right)+\\&+I_{\text{im\_nor}}\left(x,y\right)-\frac{1}{N_{\text{local}}}\times\sum_{i=-k}^{k}\sum_{j=-k}^{k}I_{\text{im\_nor}}\left(x+i,y+j\right)\end{aligned} \tag{15}$$

Here, $I_{\text{local}_{\text{contrast}}}\left(x,y\right)$ is the local mean of the image $I_{\text{im\_nor}}\left(x,y\right)$. The parameter k is the enhancement factor, typically set to 0.5. The term $\omega_{\text{edge}}\left(x,y\right)$ refers to the edge strength map. The value $\mathrm{N}_{\text{local}}$ represents the number of pixels within the sliding window, calculated as $w \times h$.

A linear weighting approach is used to merge details from different scales, prioritizing large-scale features while retaining fine local textures. In this process, the weights for the fine, base, and coarse scales correspond to different levels of image detail. The fusion formula is as follows:

$$\begin{aligned}&I_{\text{detail\_ro}}\left(x,y\right)=\omega_{\text{detail\_1}}\times I_{\text{detail\_f}}\left(x,y\right)+\\&+\omega_{\text{detail\_2}}\times I_{\text{detail\_b}}\left(x,y\right)+\omega_{\text{detail\_3}}\times I_{\text{detail\_c}}\left(x,y\right)\end{aligned} \tag{16}$$

where $\omega_{\text{detail\_1}}$, $\omega_{\text{detail\_2}}$, and $\omega_{\text{detail\_3}}$ are the weights assigned to the fine, base, and coarse scales, respectively. The weights satisfy $\omega_{\text{detail},1}+\omega_{\text{detail},2}+\omega_{\text{detail},3}=1$.

A more effective image enhancement result can be obtained by combining the outputs of local contrast enhancement and overall detail fusion using weighted addition. The exact formula is given below:

$$\begin{aligned}&I_{\text{enhance}}\left(x,y\right)=\\&\omega_{\text{con}}\times I_{\text{contrast}}\left(x,y\right)+\omega_{\text{det}}\times I_{\text{detail\_ro}}\left(x,y\right)\end{aligned} \tag{17}$$

Here, ω_{con} represents the contrast edge weight and ω_{det} represents the detail edge weight, where the sum of ω_{con} and ω_{det} is equal to 1.

Unlike prior hybrids that simply chain CLAHE and gamma, MSFIE (i) adapts dual-gamma with cosine boundary blending, (ii) sets the CLAHE clip limit from L-channel Laplacian variance, and (iii) fuses fine/base/coarse details with edge-aware local contrast to balance global brightness and local texture recovery under mixed illuminations.

4 EXPERIMENTAL SETUP

4.1 Dataset and Diversity

In this section, we initially delineate the implementation specifics. We show and analyze the experimental results, including both descriptive and numerical assessments compared to other low-light enhancement models, as well as the detailed tests of our proposed model. The investigations are performed using a collection of 150 ultra-low-light photos taken from curing barns that show settings with either no lighting at all or very little, partial lighting.

We collected 150 ultra-low-light images from multiple curing barns and batches, spanning six lighting scenarios (strong local light, reflected light, weak ambient light, weak ground light, no-light, localized light sources) and multiple camera models/resolutions. No learning-based training was performed; all methods were run with default or recommended parameters. While 150 images suffice for algorithmic benchmarking, broader generalization requires larger, multi-crop datasets and varied camera pipelines.

4.2 Implementation Details

In this study, we meticulously crafted experiments to qualitatively and quantitatively evaluate the efficacy of our algorithm. We benchmark our algorithm against Classical Algorithms methodologies (CLAHE) [16], context-based low-light image enhancement (CoLIE) [17], a dual-approach for uniform and non-uniform low-light image enhancement (ALEN) [18], a new color space for low-light image enhancement (HVI) [19], fast baselines for real-world low-light (FLOL) [20], low-light image enhancement transformer (LLIEFormer) [21], learning to enhance low-light image via zero-reference deep curve estimation (ZeroDCE++) [22], and our algorithm. To maintain equitable conditions in the comparative analysis, all implementations are executed in Python, and the experiments are conducted on a Windows 10 PC equipped with 32 GB RAM and a 2.3 GHz CPU. The parameters of our enhancement algorithm remain constant throughout all trials: the threshold for bright regions, we scale bright regions by a factor of 0.7 and dark regions by 1.3, and the convolution kernel size is 3 × 3. The bright/dark thresholds are derived from image statistics tied to Eq. (9). Scaling factors (0.7 for bright, 1.3 for dark) were selected via grid search on a small validation subset to minimize luminance distortion while maximizing Laplacian variance.

Under extremely low-light conditions, five key parameters local medium-scale detail, local fine-grained detail, local major structure, global contrast, and global detail significantly influence the brightness [23] and sharpness [24] of tobacco leaf images during enhancement. The threshold values for bright and dark regions are determined based on Eq. (9). These thresholds are applicable to a variety of scenarios, such as tobacco leaf images without light, with local light sources, with dim light, with faint ground light, with reflected light, or with partial illumination. Tab. 1 presents the effects of these five parameters on image brightness and sharpness. For different application scenarios, the sum of the three local parameters - medium-scale detail, fine-grained detail, and major structure - is set to 1, while the sum of global contrast and global detail parameters is also set to 1.

Table 1 An analysis of the relationship between five parameters, global contrast, global detail, medium-scale detail, fine-grained detail, and major structural detail and the brightness and sharpness of tobacco leaf images

Local medium-scale detail parameter	Local fine-grained detail parameter	Local primary structure parameter	Global contrast parameter	Global detail parameter	Clarity	Brightness
0.9	0.05	0.05	0.3	0.7	7852.85	131.55
0.8	0.05	0.15	0.3	0.7	7963.42	131.66
0.7	0.05	0.25	0.3	0.7	8072.85	131.76
0.6	0.05	0.35	0.3	0.7	8181.52	131.87
0.5	0.05	0.45	0.3	0.7	8289.90	131.97
0.4	0.05	0.55	0.3	0.7	8396.74	132.07
0.3	0.05	0.65	0.3	0.7	8504.71	132.17
0.2	0.05	0.75	0.3	0.7	8611.04	132.27
0.1	0.05	0.85	0.3	0.7	8716.09	132.37
0.1	0.05	0.85	0.1	0.9	8715.45	132.36
0.1	0.05	0.85	0.2	0.8	8715.47	132.34
0.1	0.05	0.85	0.3	0.7	8714.21	132.33
0.1	0.05	0.85	0.4	0.6	8713.20	132.31
0.1	0.05	0.85	0.5	0.5	8712.17	132.29
0.1	0.05	0.85	0.6	0.4	8710.69	132.28
0.1	0.05	0.85	0.7	0.3	8708.96	132.26
0.1	0.05	0.85	0.8	0.2	8706.71	132.24
0.1	0.05	0.85	0.3	0.7	9633.61	132.84
0.1	0.15	0.75	0.3	0.7	9170.38	132.60
0.1	0.25	0.65	0.3	0.7	8716.09	132.37
0.1	0.35	0.55	0.3	0.7	8270.42	132.14
0.1	0.45	0.45	0.3	0.7	7834.41	131.92
0.1	0.55	0.35	0.3	0.7	7408.28	131.70
0.1	0.65	0.25	0.3	0.7	6993.58	131.49
0.1	0.75	0.15	0.3	0.7	6589.21	131.27
0.1	0.85	0.05	0.3	0.7	6196.80	131.07

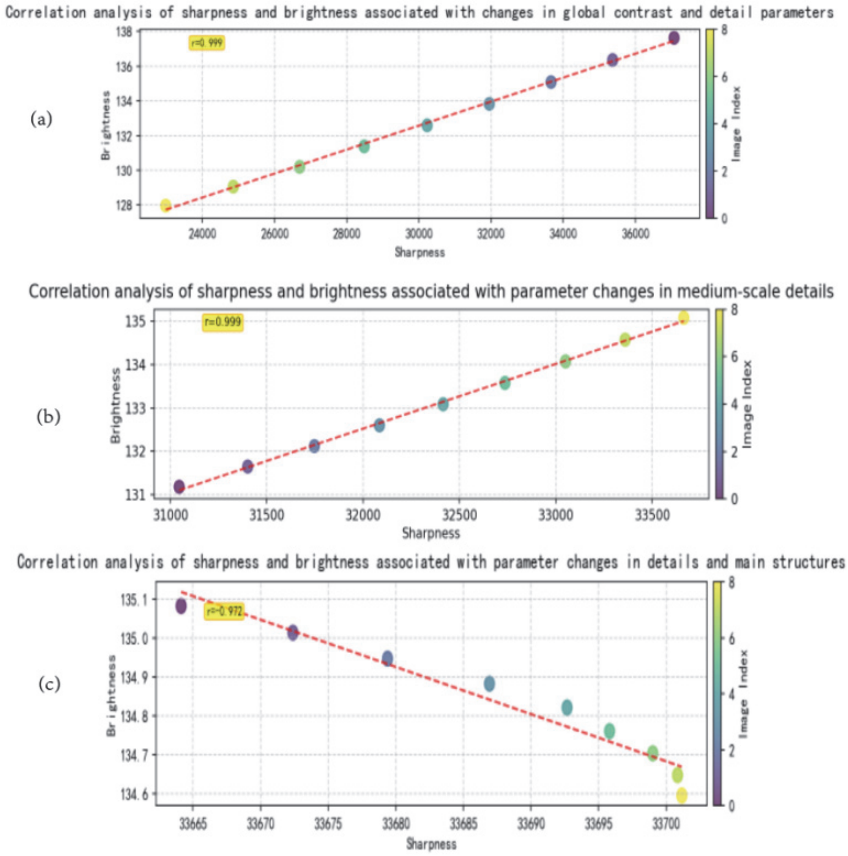

Figure 2 Five parameters - global contrast, global detail, medium-scale detail, fine detail, and major structural detail-collectively determine image brightness and sharpness

In Tab. 1, only global contrast and global detail parameters are adjustable, while the others remain constant. All parameters are positively correlated with image brightness and sharpness, as shown in Fig. 2a; as sharpness decreases, brightness also declines. When adjusting only the local medium-scale detail parameter (with other parameters held constant), a positive correlation between sharpness and brightness persists (Fig. 2b). However, when global contrast and detail are adjusted, the relationship becomes negative (Fig. 2c); brightness decreases as sharpness increases. To achieve the best image brightness and sharpness, it is important to adjust these parameters adaptively and consider the texture and noise in the original image. This approach helps improve both the clarity and accuracy of the enhanced image.

5 RESULTS
5.1 Image Enhancement Results of MSFIE

We investigated six image settings: strong local light, reflected light, weak ambient light, weak ground light, images without light and images with localized light sources. The MSFIE algorithm's numerical results are summarized in Tab. 2, which also shows the performance gains. Images before and after enhancement are visually compared in Fig. 3.

The original images contain histograms grouped at low pixel values, which indicates low brightness and poor clarity, as seen in Fig. 3 and Tab. 2. Tab. 2 further shows that these images usually have sharpness below130, brightness less than 17, and information entropy under 5, which all point to limited detail. Panels (c) and (d) of Fig. 3 demonstrate observable visual enhancements after augmentation. To show more information, the histograms cover a wider range of pixel values, and both brightness and contrast increase. As shown in Tab. 2, the enhanced images attain brightness levels above 110 and sharpness levels above 7,930. For example, brightness increased from 2.45 to 133.75 (0-255 scale), and Laplacian-based sharpness from 72.23 to 29,856.22 raw units. All enhanced images show at least 1.5 times more detail when the information entropy value is above 7.3. PSNR values higher than 5.5 indicate improved image quality. The updated histograms also highlight changes in brightness across the color channels. Overall, the MSFIE algorithm greatly enhances image quality, contrast, brightness, and detail, making it a great option for practical applications.

Table 2 Quantitative comparison of brightness, information entropy, and PSNR before and after enhancement across six images

Image File	Original Image Clarity	Enhanced Image Clarity	Original Image Brightness	Enhanced Image Brightness	Original Information Entropy	Enhanced Information Entropy	PSNR
Image1	72.233	29856.220	2.450	133.747	2.470	7.692	6.336
Image2	128.941	7930.441	14.770	131.017	4.573	7.828	6.582
Image3	5.007	23070.520	2.281	114.487	2.512	7.390	7.253
Image4	115.382	29935.687	16.251	137.658	4.413	7.851	6.309
Image5	49.988	29239.506	14.699	140.963	4.288	7.841	6.213
Image6	5.037	30116.383	2.552	140.504	2.582	7.848	5.672

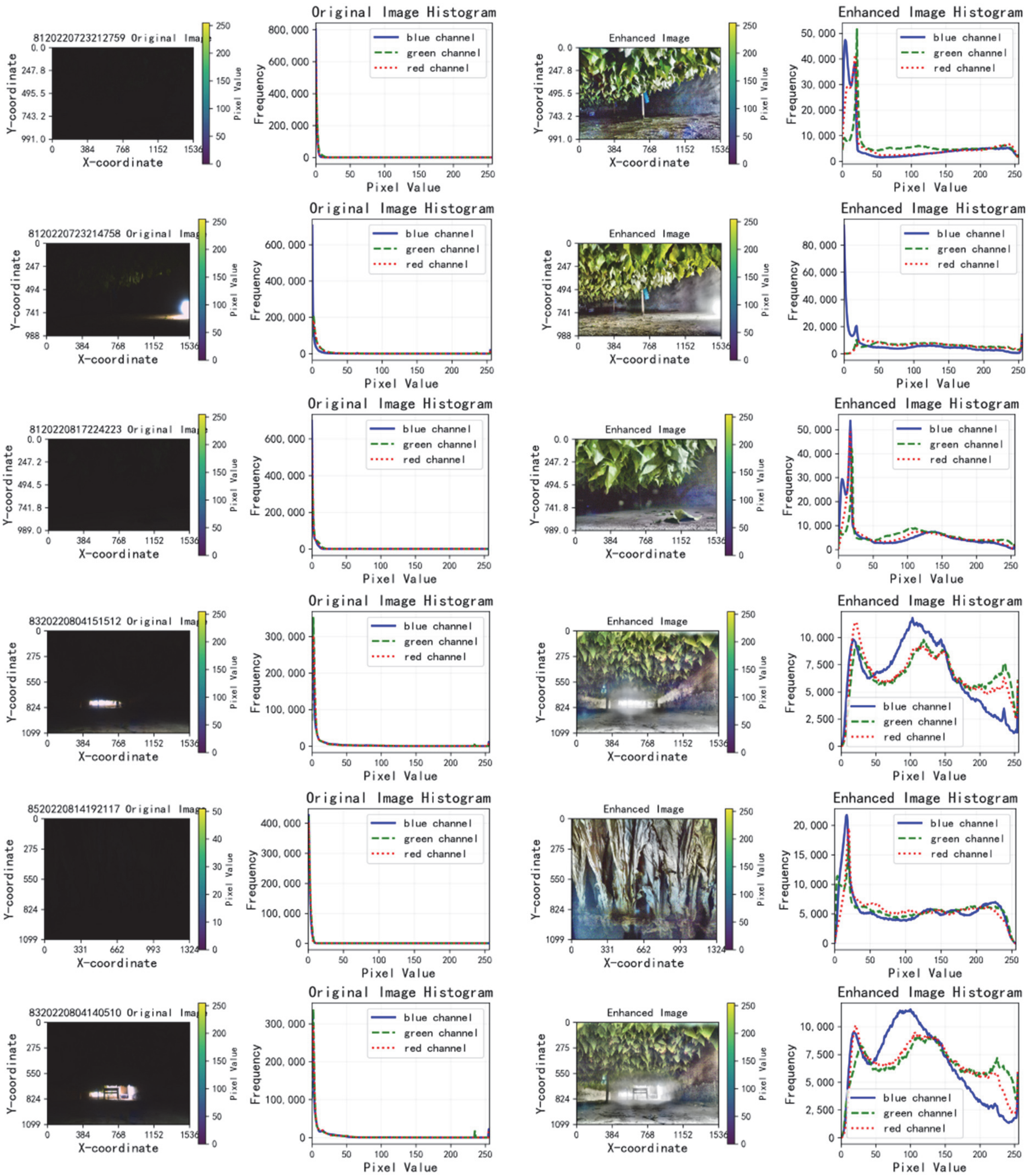

(a) (b) (c) (d)

Figure 3 Original and enhanced images with corresponding histograms for six low-light scenarios. A comparative analysis of our algorithm's efficacy in augmenting image brightness and contrast. The first and third rows present the original images captured in severely low-light conditions alongside their histograms. The subsequent second and fourth rows exhibit the enhanced images with their corresponding histograms. The subsequent second and fourth rows exhibit the enhanced images with their corresponding histograms. We show six common examples of low-light image improvement, along with histogram representations of the resulting images. Column (a) displays the initial low-light photos. Column (b) displays the original extremely low-light photos' histogram distribution. Column (c) displays the improved images after processing them. Column (d) displays the improved images' histogram properties

5.2 MSFIE vs. Existing Algorithms

Fig. 4 compares the enhancement results of various algorithms on tobacco leaf images under three conditions: extremely low illumination (first column), localized lighting (third column), and strong local illumination (fifth column). In the original images, pixel values are concentrated at the low end, with maximum values of 1,402,912, 1,441,725, and 609,727, indicating low brightness and limited detail. Although CLAHE improves brightness and sharpness and creates a more even pixel distribution (maximum values: 174,493; 431,578; 41,574), it still has issues with overexposure, detail loss, color distortion, and artifacts. CoLIE also has trouble; images appear gloomy, with sporadic blurring and little detail recovery because its maximum pixel values (1,041,994; 1,210,278; 297,221) are still low. ALEN balances brightness (highest values: 898,437; 1,573,955; 1,174,232) but improves detail only somewhat and distorts color. CIDNet somewhat improves pixel distribution (maximum: 302,536; 217,984; 69,783), but it has little effect in dark areas and typically over-enhances bright parts, LLIEFormer (maximum: 173,436; 50,986; 29,018) RUAS produces dark photos with poor detail and color distortion. FLOL produces low-contrast yellowish photos (maximum: 155,750; 108,557; 115,455) with most pixels in the low range. LLIEFormer produces low-contrast yellowish photos (maximum: 359,010; 108,358; 55,214) with most pixels in the low range. ZeroDCE++ works well in low light, however tobacco leaf photos are dark and lack detail (maximum: 920,118; 1,114,858; 233,546).

Instead, MSFIE creates a more equal pixel distribution with lower maximum values (79,643; 219,340; 24,692), improving brightness and detail. Histogram research shows that MSFIE produces images with superior resolution, brightness, and natural color without distortion or artifacts. It also effectively reduces local overexposure. CLAHE alone may over-amplify noise and clip highlights; ZeroDCE++ can leave color casts under severe darkness; transformer-based baselines may struggle without domain-specific data. MSFIE's dual-gamma equalizes dynamic range locally, Laplacian-guided CLAHE elevates detail-rich regions, and edge-aware multi-scale fusion restores leaf veins without boosting flat-region noise, yielding more uniform histograms and improved local contrast.

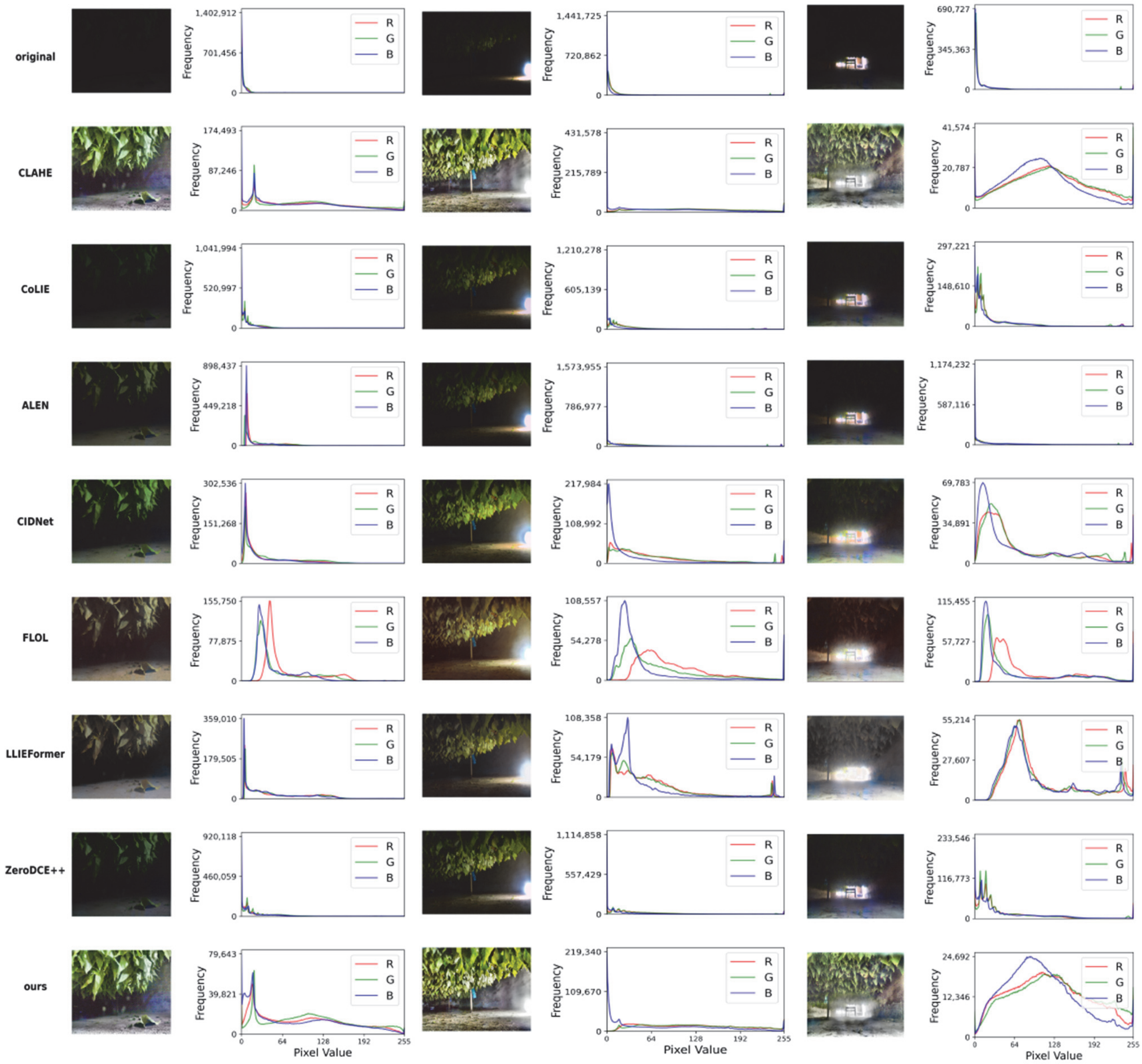

Figure 4 The efficacy of the proposed algorithm was rigorously evaluated against the most prevalent low-light enhancement methodologies through empirical analysis on completely dark low-light images

Fig. 5 further evaluates local regions, focusing on color accuracy, detail recovery, and pixel distribution. Once more, the original photos had little detail and low pixel values (up to 30,000). Although CLAHE increases brightness and sharpness (up to 30,000; 30,000; and 30,000), it often causes overexposure, color distortion, feature loss, and visible artifacts. CoLIE produces a more balanced pixel distribution (up to 30,000, 30,000, 7,500), but images remain dim and lack detail, especially in low-light scenes. ALEN (up to 30,000, 40,000, and 30,000) only slightly enhances dark regions and may introduce artifacts in bright spots. For images with ultra low luminance (approximately 4,000-30,000 in the raw intensity domain), CIDNet produces limited detail enhancement, and the locally enhanced regions exhibit color distortions and artifacts. With the majority of pixels in the lower range, FLOL is unable to restore color and detail (maximum: 1,500; 3,000; 75,000). LLIEFormer enhances under low light, but fails to recover detail and color for tobacco leaves (maximum: 4,000; 6,000; 20,000). ZeroDCE++ enhances under low light, but fails to recover detail and color for tobacco leaves (maximum: 30,000; 30,000; 40,000). Most pixels remain at low values. MSFIE outperforms all other methods, with lower and more evenly distributed pixel values (10,000; 8,000; 30,000) and more dispersed histograms. It excels in restoring natural color, recovering fine details, and suppressing artifacts under strong lighting. Both subjective evaluation and quantitative metrics confirm MSFIE's stable, superior performance under complex lighting and specific enhancement tasks.

Tab. 3 quantitatively compares MSFIE with seven mainstream algorithms using several image quality metrics. MSFIE achieves the highest mean luminance (120.33) and mean luminance distortion (7.67), resulting in optimal brightness and better detail. MSFIE's luminance skewness **Pogreška! Izvor reference nije pronađen.** of 0.16 indicates natural light distribution. The image has the mean contrast standard deviation (64.55) and total contrast (145.22). These improvements enhance visual clarity and tone transitions. MSFIE captures the most picture detail, as seen by its top information entropy index (64.55) and shannon entropy (7.84). It has the local contrast (10.56) for fine details. The algorithm's highest Laplacian variance values (18,007.41) improve sharpness and clarity. The MSFIE'speak signal-to-noise Ratio is 6.52; peak signal-to-noise ratio standard deviation is 0.55 and mean absolute error standard deviation is 7.24, indicating realistic photographs with accurate color. Maximum frequency domain clarity (47,133.01) enhances detail. MSFIE outperforms other algorithms in contrast, sharpness, and image clarity, boosting detail, noise reduction, and natural look.

To streamline reporting and avoid redundancy, we note that mean variance of Laplacian (MVL) is effectively interchangeable with other Laplacian-based sharpness indices; therefore, we present MVL in the main text for brevity and move the remaining sharpness variants to the supplement. Moreover, paired Wilcoxon signed-rank tests across images confirm that MSFIE significantly outperforms the strongest baseline in mean luminance ($p < 0.01$), MVL ($p < 0.01$), and local contrast ($p < 0.05$), supporting the robustness of the above improvements.

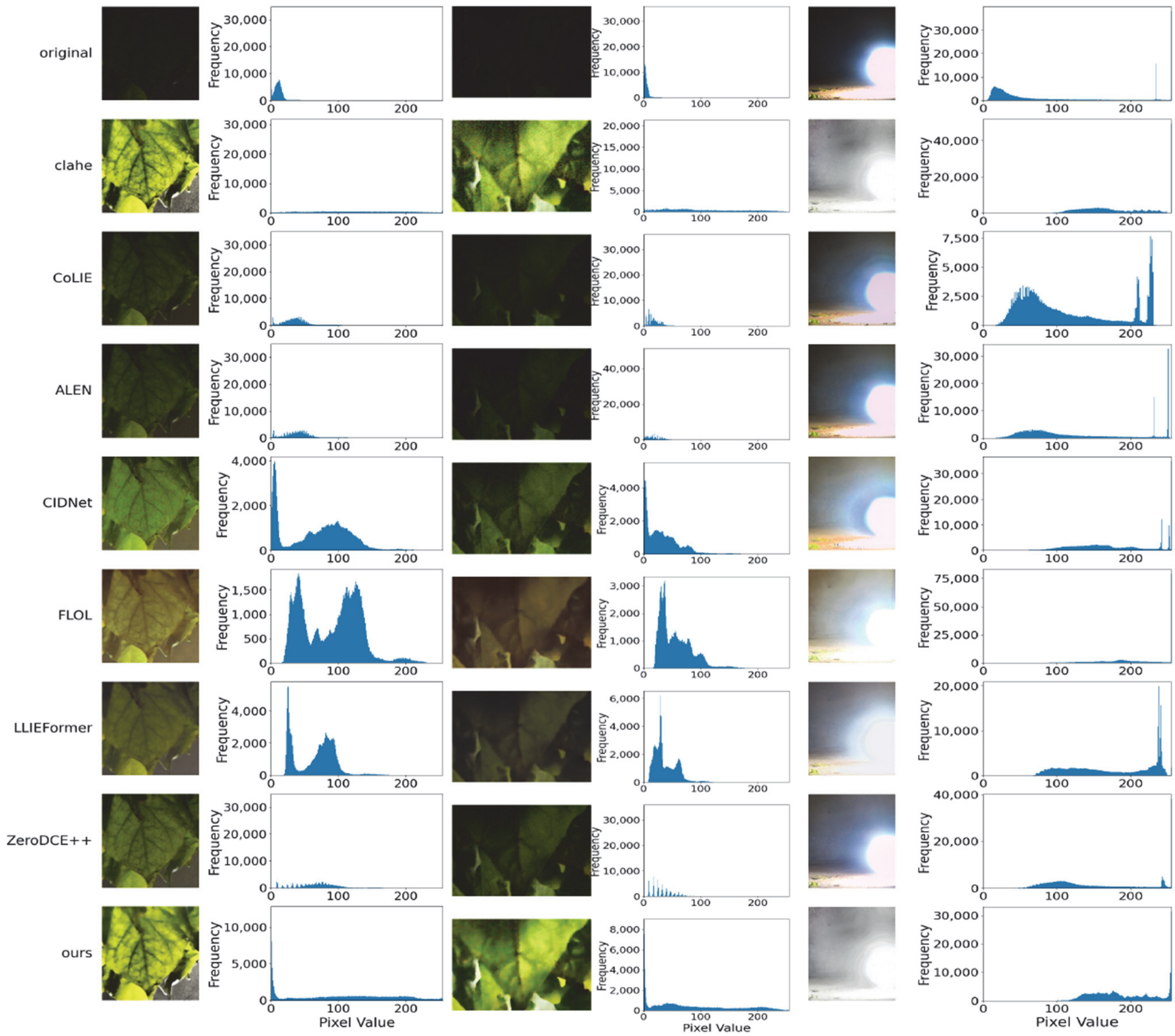

Figure 5 The efficacy of the proposed algorithm was rigorously evaluated against the most prevalent low-light enhancement methodologies through empirical analysis on completely dark low-light images

Table 3 Performance comparison of eight algorithms on Mean Luminance (ML) [25], Luminance Skewness (LS), Contrast (CT), Shannon Entropy (SH), Local Contrast (LC), Mean Naturalness (MN), Mean Luminance Distortion (MLD), Mean Contrast Standard Deviation (MCSD), Mean Variance of Laplacian (MVL), Peak Signal-to-Noise Ratio (PSNR), Peak Signal-to-Noise Ratio Standard Deviation (PSNRSD), Mean Absolute Error Standard Deviation (MAESD), Frequency-domain Sharpness Mean (FMSM), Frequency-domain Sharpness Standard Deviation (FMSMSD), Enhancement Index (EI)

Algorithm	CLAHE	CoLIE	ALEN	CIDNet	FLOL	LLIEFormer	ZeroDCE++	Ours
ML	118.30	39.78	52.99	56.81	87.67	77.30	56.58	**120.33**
MLD	9.70	88.22	75.01	71.44	40.33	50.95	71.42	**7.67**
LS	0.18	1.74	1.32	1.17	0.87	0.94	1.14	**0.16**
MCSD	62.94	31.32	39.04	46.87	52.95	48.72	38.36	**64.55**
TC	139.20	21.50	22.45	33.39	24.26	18.65	29.65	**145.22**
EI	62.94	31.31	39.02	46.86	52.95	48.72	38.35	**64.55**
SH	7.78	6.13	6.36	6.82	7.11	7.02	6.62	**7.84**
LC	10.41	9.14	9.13	10.22	10.10	9.70	9.76	**10.56**
MN	33.56	15.63	16.95	21.03	19.87	17.40	18.35	**34.89**
MVL	16316.03	262.00	149.27	177.89	102.82	63.41	387.66	**18007.41**
PSNR	6.69	20.12	16.21	14.09	9.93	11.99	15.20	**6.52**
PSNRSD	0.55	4.53	4.16	2.17	1.64	4.03	3.56	**0.55**
MAESD	7.41	16.28	22.38	12.42	15.50	26.53	17.82	**7.24**
FMSM	47081.19	41927.52	42550.28	43225.55	43565.23	43432.28	43015.66	**47133.01**
FMSMSD	402.22	1722.29	1384.15	1054.56	1038.27	735.31	1613.40	**395.98**

6 DISCUSSION

MSFIE reduces local overexposure, restores shadow textures, and yields natural color under mixed illumination, enabling more reliable remote visual inspection of curing stages. Fig. 2 compares MSFIE with seven leading algorithms under very low illumination. MSFIE performs better than seven top algorithms in very low light when looking at important measures like average brightness, brightness variation, contrast, information richness, local contrast, how natural the image looks, brightness errors, sharpness, average contrast, overall error, local contrast improvement, noise reduction, and sharpness in different frequencies. The algorithm excels at bringing back textures and details in dark areas. As shown in Fig. 4, MSFIE restores the natural color of leaves, reduces overexposed spots, preserves leaf veins, balances lighting, and increases brightness in low-light images.

Tab. 3 presents performance metrics that validate the efficacy of our proposed MSFIE against existing methods. Achieving the highest mean luminance (ML) of 120.33, our algorithm significantly enhances image brightness. Its balanced contrast is evidenced by a contrast (CT) of 145.22 and a low luminance skewness (LS) of 0.16, indicating effective illumination without overexposure. Robustness is further demonstrated by a high peak signal-to-noise ratio (PSNR) of 6.52 and the lowest PSNR standard deviation (PSNRSD) of 0.55, signifying consistent image quality. The mean absolute error standard deviation (MAESD) of 7.24 underscores the algorithm's error reduction precision. Notably, the highest frame mean squared error (FMSE) of 47133.01 indicates superior computational efficiency, suggesting faster processing. Collectively, these findings affirm that our algorithm provides a comprehensive solution for image enhancement, effectively balancing quality, consistency, and performance, rendering it highly applicable for practical use.

MSFIE can be embedded in edge devices connected to curing-barn cameras to enable real-time stage monitoring, thereby reducing manual inspection and improving batch consistency; however, this study has several limitations - including a relatively small dataset, absence of real-time profiling on edge hardware, nontrivial multi-scale processing cost, and potential over-enhancement near extreme specular highlights - that motivate future work on (i) real-time deployment and optimization on embedded platforms, (ii) broader evaluation across multiple crops and heterogeneous camera pipelines, (iii) hybridization with transformer/GAN-based denoising and color constancy, and (iv) semi/self-supervised learning with synthetic augmentation to improve generalization and robustness.

7 CONCLUSION

This paper presents a Multi-Scale Fusion-Based Image Enhancement (MSFIE) framework designed to improve photos of tobacco leaves taken in very low light conditions. We presented MSFIE, a multi-scale fusion approach that integrates adaptive dual-gamma correction, Laplacian-guided CLAHE, and edge-aware multi-scale detail fusion to enhance ultra-low-light agricultural images. MSFIE improves brightness uniformity, detail preservation, and color fidelity across diverse kiln lighting conditions. Embedded within IoT edge units connected to barn cameras, MSFIE can support real-time stage monitoring and reduce reliance on manual inspection.

Acknowledgements

This research was funded by Science and Technology Planning Project of Sichuan Province, China (Grant nos. 2024YFHZ0139 and 2023YFN0094) and the Doctoral Research Start-up Project of Xichang University (Grant no. YBZ202209, and YBZ202106).

8 REFERENCES

[1] Huang, J. & Jin, Z. (2024). Enhanced image denoising with diffusion probability and dictionary learning adaptation. *Tehnički vjesnik - Technical Gazette*, *31*(3), 774-783. https://doi.org/10.17559/tv-20230808000859

[2] Petrescu, M., Ştefan, M.-C., Panagoreţ, A. A., Croitoru, I. O., Chiriţă, S., & Steriopol, B. C. (2024). Route planning and machine learning algorithms for sensor-equipped autonomous vehicles in agriculture. *Studies in Informatics and Control*, *33*(4), 105-112. https://doi.org/10.24846/v33i4y202410

[3] Chen, Z., Yan, L., Wang, C., & Ye, Z. (2024). Improved discriminator network based on residual network for person image synthesis. *Tehnički vjesnik - Technical Gazette*, *31*(6), 1815-1825. https://doi.org/10.17559/tv-20240416001467

[4] Vesselenyi, T., Dzitac, I., Dzitac, S., & Vaida, V. (2008). Surface roughness image analysis using quasi-fractal characteristics and fuzzy clustering methods. *International Journal of Computers Communications & Control*, *3*(3), 304-316. https://doi.org/10.15837/ijccc.2008.3.2398

[5] Guo, W. M., Zhao, H., Zheng, J. M., Zhang, Y. L., Liu, J. J., Wang, J. W., Wang, A. G., Cai, X. J., Xu, C. Y., & Zheng, F. (2021). Big data analysis on flue-curing process of tobacco leaves in Henan based on data acquisition via internet of things (IoTs). *Tobacco Science & Technology*, *54*(9), 11-18, 39. https://doi.org/10.16135/j.issn1002-0861.2021.0297

[6] Jiang, Z. Y., Zhu, S. P., Feng, C., Wang, T., & Li, J. X. (2023). Research on high-precision lightweight model for tobacco leaves baking stage identification. *Acta Tabacaria Sinica*, *29*(1). https://doi.org/10.16472/j.chinatobacco.2022.T0135

[7] Peng, D. X., Zhen, T., & Li, Z. H. (2023). Survey of research methods for low light image enhancement. *Computer Engineering and Applications*, *59*(18). https://doi.org/10.16472/j.chinatobacco.2022.T0135

[8] Yang, S. H., He, X., Cao, H., & Cui, W. L. (2011). Double-plateaus histogram enhancement algorithm for low-light-level night vision image. *Journal of Convergence Information Technology*. https://doi.org/10.4156/jcit.vol6.issue1.29

[9] Wang, X. X., Yi, R., Sun, M. Y., & Zhang, Z. Z. (2024). Low-light image enhancement algorithm based on improved multi-scale Retinex with adaptive brightness compensation. *2024 27th International Conference on Computer Supported Cooperative Work in Design (CSCWD)*. https://doi.org/10.1109/CSCWD61410.2024.10580802

[10] Wang, S., Lu, Q. W., Peng, B. X., Nie, Y. H., & Tao, Q. C. (2025). DPEC: Dual-path error compensation method for enhanced low-light image clarity. *Neurocomputing*, *637*. https://doi.org/10.1016/j.neucom.2025.129980

[11] Sun, Z. W., Chen, Z. Q., Pei, Q. Q., & Lai, J. A. (2023). Low-light image enhancement network based on gamma correction and multi-scale attention mechanism. 2023 IEEE 7th Information Technology and Mechatronics *Engineering Conference (ITOEC)*, 772-772. https://doi.org/10.1109/ITOEC57671.2023.10291706

[12] Zhao, X. P. & Li, L. (2024). A low-light-level image enhancement algorithm combining Retinex and Transformer. *2024 4th International Conference on Artificial Intelligence, Robotics, and Communication (ICAIRC)*. https://doi.org/10.1117/12.3029685

[13] Brateanu, A., Balmez, R., Avram, A., Orhei, C., &Ancuti, C. (2025). LYT-NET: Lightweight YUV Transformer-based network for low-light image enhancement. *IEEE Signal Processing Letters*, *32*, 2065-2069. https://doi.org/10.1109/LSP.2025.3563125

[14] Dong, Q., Wang, Z., Li, M., Gao, J., Chen, S., Shu, Z., Xin, S., Tu, C., & Wang, W. (2024). Laplacian2Mesh: Laplacian-based mesh understanding. *IEEE Transactions on Visualization and Computer Graphics*, *30*(7), 4349-4361. https://doi.org/10.1109/TVCG.2023.3259044

[15] Wu, T., Wang, L., & Zhu, J. (2021). Image edge detection based on Sobel with morphology. *Proceedings of the 2021 IEEE 5th Information Technology, Networking, Electronic and Automation Control Conference (ITNEC)*, 1216-1220. https://doi.org/10.1109/ITNEC52019.2021.9586895

[16] Mohammed, I. M. & Mat Isa, N. A. (2025). Contrast limited adaptive local histogram equalization method for poor contrast image enhancement. *IEEE Access*, *13*, 62600-62632. https://doi.org/10.1109/ACCESS.2025.3558506

[17] Chobola, T., Liu, Y., Zhang, H., Schnabel, J. A., & Peng, T. (2024). Fast context-based low-light image enhancement via neural implicit representations. *Springer Nature Switzerland*. https://doi.org/10.1007/978-3-031-73016-0_24

[18] Perez-Zarate, E., Ramos-Soto, O., Liu, C., Oliva, D., & Perez-Cisneros, M. (2024). ALEN: A dual-approach for uniform and non-uniform low-light image enhancement. *Applied Sciences*. https://doi.org/10.1007/s00530-025-01812-7

[19] Yan, Q. S., Feng, Y. X., Zhang, C., Pang, G. S., Shi, K. B., Wu, P., Dong, W., Sun, J. Q., & Zhang, Y. N. (2025). HVI: A new color space for low-light image enhancement. *2025 IEEE/CVF Conference on Computer Vision and Pattern Recognition (CVPR)*. https://doi.org/10.1109/CVPR52734.2025.00533

[20] Benito, J. C., Feijoo, D., García, A., & Conde, M. V. (2025). FLOL: Fast baselines for real-world low-light enhancement. CoRR. https://doi.org/10.48550/arXiv.2501.09718

[21] Yi, X., Wang, Y., Zhao, Y., Yan, J., & Zhang, W. (2023). LLieformer: A low-light image enhancement transformer network with a degraded restoration model. *2023 IEEE International Conference on Image Processing (ICIP)*. https://doi.org/10.1109/ICIP49359.2023.10222840

[22] Li, C., Guo, C., & Chen, C. L. (2021). Learning to enhance low-light image via zero-reference deep curve estimation. *IEEE Transactions on Pattern Analysis and Machine Intelligence*, *44*(5), 555. https://doi.org/10.1109/TPAMI.2021.3063604

[23] Wang, H., Peng, L., Sun, Y., Wan, Z., Wang, Y., & Cao, Y. (2024). Brightness perceiving for recursive low-light image enhancement. *IEEE Transactions on Artificial Intelligence*, *5*(6), 3034-3045. https://doi.org/10.1109/TAI.2023.3339092

[24] Zhan, Y. & Zhang, R. (2018). No-reference image sharpness assessment based on maximum gradient and variability of gradients. *IEEE Transactions on Multimedia*, *20*(7), 1796-1808. https://doi.org/10.1109/TMM.2017.2780770

[25] Gubu, L. & Hilmi, M. R. (2024). Beyond mean-variance Markowitz portfolio selection: A comparison of mean-variance-skewness-kurtosis model and robust mean-variance model. *Economic Computation and Economic Cybernetics Studies and Research*, *58*(1), 298-313. https://doi.org/10.24818/18423264/58.1.24.19

Contact information:

Jun LI
(Corresponding author)
School of Information Technology, Xichang University,
Key Laboratory of Liangshan Agriculture Digital Transformation of Sichuan Provincial Education Department,
Xichang 615013, China
E-mail: lijun@xcc.edu.cn

Zhou WEI
Xichang Cigarette Factory, China Tobacco Sichuan Industrial Co. Ltd.,
Xichang, China
Xichang, Sichuan, 618400, China
E-mail: zhouwei@sctobacco.com

Yining SONG
International Telecommunication Union,
1211 Geneva, Switzerland
E-mail: songyining1225@gmail.com

Shiqiong CHEN
School of Information Technology, Xichang University,
Key Laboratory of Liangshan Agriculture Digital Transformation of Sichuan Provincial Education Department,
Xichang 615013, China
E-mail: 79602769@qq.com

Miao YU
School of Information Technology, Xichang University,
Key Laboratory of Liangshan Agriculture Digital Transformation of Sichuan Provincial Education Department,
Xichang 615013, China
E-mail: 18583669695@163.com

Wenfeng WANG
School of Information Technology, Xichang University,
Key Laboratory of Liangshan Agriculture Digital Transformation of Sichuan Provincial Education Department,
Xichang 615013, China
E-mail: 1085990062@qq.com

Chenping ZENG
School of Information Technology, Xichang University,
Key Laboratory of Liangshan Agriculture Digital Transformation of Sichuan Provincial Education Department,
Xichang 615013, China
E-mail: zengchenping@xcc.edu.cn

Yanmeng CHEN
School of Information Technology, Xichang University,
Key Laboratory of Liangshan Agriculture Digital Transformation of Sichuan Provincial Education Department,
Xichang 615013, China
E-mail: 3401254781@qq.com